Journal of Applied Polymer Science

Study on the Poly(3-hydroxybutyrate-*co*-4-hydroxybutyrate)-Based Nanocomposites Reinforced by Surface Modified Nanocrystalline Cellulose

Rui Zhang,[1,2] Changjiang Zhu,[1] Xueying Shan,[3] Jing Xia,[1] Qing Zhu,[1] Yuan Hu[3]

[1]Department of Materials Science and Engineering, College of Chemical Engineering, Nanjing Forestry University, Nanjing, Jiangsu 210037, People's Republic of China

[2]Jiangsu Key Lab of Biomass-based Green Fuels and Chemicals, Nanjing Forestry University, Nanjing, Jiangsu 210037, People's Republic of China

[3]Suzhou Key Laboratory of Urban Public Safety, Suzhou Institute of University of Science and Technology of China, Suzhou, Jiangsu 215123, People's Republic of China

Correspondence to: R. Zhang (E-mail: zhrlm@ustc.edu)

ABSTRACT: As a kind of reinforcing agent, the application of nanocrystalline cellulose (NCC) is widely limited in hydrophobic polymers owing to its rich hydroxyl surface. In this study, NCC was modified with lauric acid/*p*-toluensulfonyl chloride mixture, then the modified nanocrystalline cellulose (mNCC) was incorporated into biopolyester poly(3-hydroxybutyrate-*co*-4-hydroxybutyrate) (P(3,4)HB) by solution casting to prepare P(3,4)HB/mNCC nanocomposites. The prepared mNCC and P(3,4)HB/mNCC nanocomposites were characterized by Fourier transform-infrared, X-ray diffraction, contact angle test, transmission electron microscopy, scanning electron microscopy, differential scanning calorimetric, polarized optical microscope, dynamic mechanical analysis, and thermogravimetric analysis. The results show that the crystallinity and mechanical properties of P(3,4)HB are greatly improved due to the fact that NCC can be modified successfully and the mNCC can distribute uniformly in nanoscale in the matrix with good compatibility along the interface. © 2013 Wiley Periodicals, Inc. J. Appl. Polym. Sci. 130: 2015–2022, 2013

KEYWORDS: cellulose and other wood products; composites; nanoparticles; nanowires and nanocrystals; thermal properties; mechanical properties

Received 28 February 2013; accepted 9 April 2013; Published online 14 May 2013

DOI: 10.1002/app.39383

INTRODUCTION

With the severe environmental issues and exhausted petrochemicals, biopolymers derived from renewable resources have attracted a great deal of interest and been considered as promising alternatives to general plastics. Polyhydroxyalkanoates (PHAs) are typical representative of the biopolymers, which are synthesized and accumulated as intracellular carbon and energy storage material by many bacteria.[1] The PHAs mainly represented by the homopolymers and copolymers of poly(3-hydroxybutyrate) (PHB). Owing to the outstanding properties, such as biodegrability, biocompatibility, and excellent mechanical performance,[2] PHB has wide application prospect on food packing, agriculture, and tissue engineering fields. Nevertheless, the fatal weakness, such as high melting temperature, high crystallinity, and large spherulitic structures with slow growth result in brittleness and low thermal stability,[3] greatly limit the application of PHB. When adding a comonomer unit 4-hydroxybutyrate, poly(3-hydroxybutyrate-*co*-4-hydroxybutyrate) (P(3,4)HB) can be fabricated. P(3,4)HB has lower melt temperature and degree of crystallinity compared with PHB.[4] Although P(3,4)HB is found to be more suitable for the industrial application, the other disadvantages including slow crystallization rate, poor mechanical properties also limit its further application in some particular areas. And there is few work that has been reported about overcoming the drawbacks of P(3,4)HB. In our previous work,[5] we applied cobalt–aluminum layered double hydroxide (LDH) as nanofiller to prepare P(3,4)HB/LDH nanocomposites. The thermal stability, thermal combustion, and thermomechanical properties for these nanocomposites were remarkably enhanced with small amount of LDH.

Nanocrystalline cellulose (NCC), a kind of polymer reinforcing agent, is needle-like elementary crystallite, which derives from the most abundant renewable resource in nature. In the past few years, much attention has been focused on NCC due to its appealing intrinsic properties including nanoscale dimensions (length 200–400 nm, diameter <10 nm),[6] high surface area,

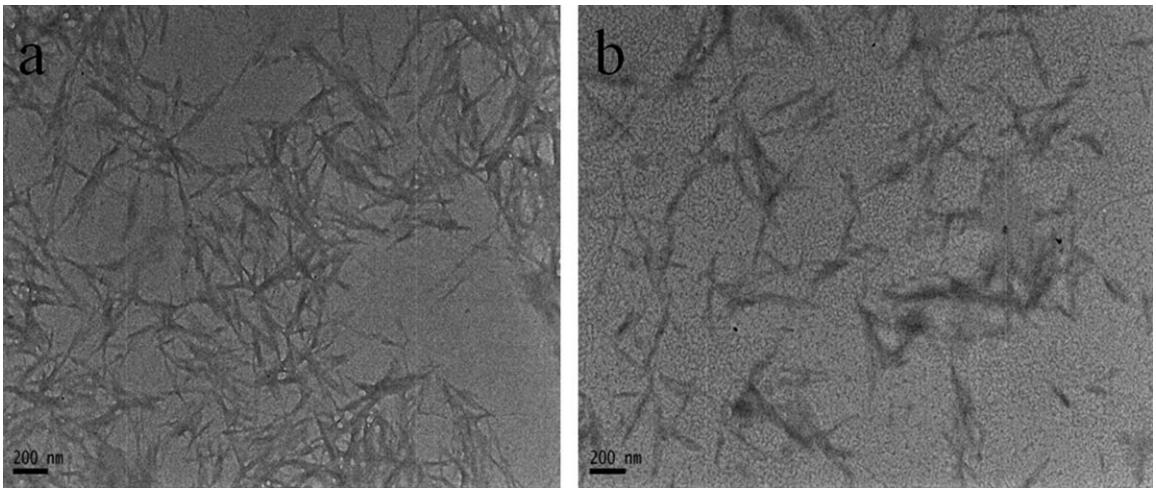

Figure 1. TEM micrographs of (a) NCC and (b) mNCC.

high Young's modulus,[7] low density, as well as being available, renewable, and biodegradable.[8] Therefore, NCC has been widely applied to reinforce polymer matrices, such as polypropylene,[9] poly(vinyl chloride),[10] polycaprolactone (PCL),[11] poly(lactic acid),[12,13] and polyurethane,[14] etc. These studies showed that NCC has certain reinforcing effect on the polymers. However, the dispersibility of NCC in the matrix and the compatibility between NCC and the matrix still need to be improved. So, a lot of work has been done to modify the hydrophilic surface of NCC, such as graft polymerization,[15–17] silylation,[18–20] acylation,[21,22] and the use of surfactants.[23,24]

In this study, we applied a simple and effective method to modify NCC and then incorporate it into P(3,4)HB to prepare P(3,4)HB based environmentally friendly nanocomposites. As far as we know, it is the first time to study P(3,4)HB based nanocomposites reinforced by surface modified NCC. It is supposed that substituted alkyl chains on NCC could greatly increase its hydrophobicity. As a result, the modified nanocrystalline cellulose (mNCC) could disperse homogenously in organic solvent without aggregation and could be incorporated into P(3,4)HB effectively. It is also supposed that strong interfacial adhesion could be created between mNCC and the matrix in the nanocomposites. The microstructure and properties of NCC and mNCC were characterized by Fourier transform-infrared (FT-IR), X-ray diffraction (XRD), transmission electron microscopy (TEM), and contact angle measurements. The microstructure and properties of the resulting nanocomposites were characterized by scanning electron microscopy (SEM), TEM, differential scanning calorimetric (DSC), polarized optical microscope (POM), dynamic mechanical analysis (DMA), and thermogravimetric analysis (TGA).

EXPERIMENTAL

Materials

P(3,4)HB containing 5% 4HB content was purchased from Tianjin Green Bio-science Co., Ltd. (Tianjin, China) with a melt flow index (MFI) of 3 g/10 min (based on ASTM 1238-906; 2.1 kg loaded at 170°C). Microcrystalline cellulose (MCC), lauric acid, *p*-toluensulfonyl chloride (Tos-Cl), pyridine, sulfuric acid (H_2SO_4), *N*,*N*-dimethylformamide (DMF), acetone, chloroform, ethanol were commercial products of the China Medicine (Group) Shanghai Chemical Reagent Corporation (Shanghai, China) and they were used without further purification.

Preparation of NCC

NCC was prepared as described in the literature.[6] MCC powder was hydrolyzed by sulfuric acid (63.5% w/w) for 130 min at 44°C with continuous stirring. Then the suspension was washed with deionized water by repeated centrifuge and sonication cycles. Finally, the suspension was filtered using dialysis with deionized water until the wash water maintained at constant PH and then freeze-dried for further use.

Surface Modification of NCC

Freeze-dried NCC (1 g) and DMF (30 mL) were added to a 250 mL flask, treated by 30 min of sonication. A certain amount of TsCl and pyridine were added to the NCC/DMF suspension with stirring, nirtrogen purging, and reflux condenser. Same molar number of lauric acid was dissolved in 10 mL DMF and dripped into the mixture slowly. The reaction was kept at 80°C for 12 h. After the reaction, the mixture was filtered and washed with ethanol and acetone, and extracted with methanol by soxhlet. Finally, the obtained mNCC was dried in vacuum oven at 50°C for 24 h.

Preparation of P(3,4)HB/mNCC Nanocomposites

A certain amount of dried P(3,4)HB powder and desired amount of mNCC was added to 50 mL chloroform. The mixture was treated with continuous stirring and sonication to make P(3,4)HB completely dissolved and mNCC uniformly dispersed. Then the suspension was casted into a Teflon mold and

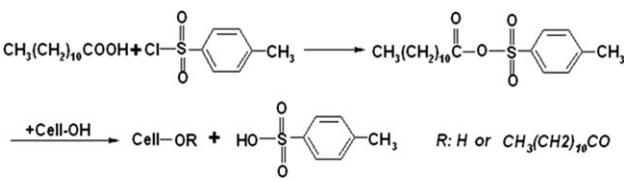

Figure 2. Schematic plot of NCC surface esterification.

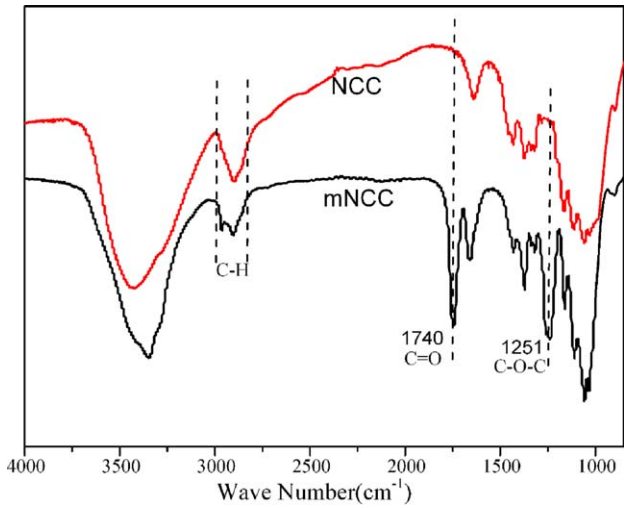

Figure 3. FT-IR spectra of NCC and mNCC. [Color figure can be viewed in the online issue, which is available at wileyonlinelibrary.com.]

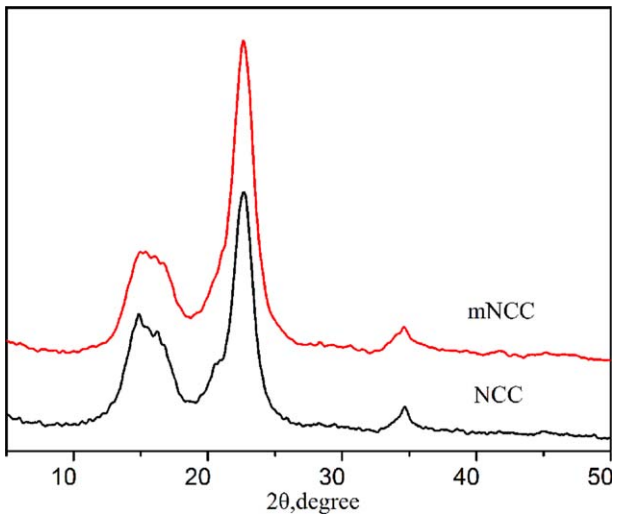

Figure 4. X-ray diffraction patterns of NCC and mNCC. [Color figure can be viewed in the online issue, which is available at wileyonlinelibrary.com.]

evaporated overnight at ambient temperature to get P(3,4)HB/mNCC nanocomposite film with a thickness of about 0.5 mm.

Measurements

FT-IR measurements were performed with Nicolet 6700 FT-IR spectrophotometer (Nicolet Instruments) using thin KBr disc.

X-ray diffraction (XRD) experiments were performed on dried NCC and mNCC powder, on a Japan Rigaku D/max-Ra X-ray diffractometer with Cu-K_α radiation(λ = 0.1542 nm) in the range of 3° to 60°.

TEM was carried out on a JEM-100SX transmission electron microscopy (JEOL, Tokyo, Japan) with an acceleration voltage of 100 kV. To examine NCC or mNCC, a droplet of the diluted suspension was dripped on a copper grid. To examine the nanocomposites, the samples were cut into ultrathin slices at room temperature with an ultramicrotome (Ultraacut-1, UK) equipped with a diamond knife. The slices were subsequently stained with 2 wt % osmic acid for 30 min.

Contact angle measurements were performed at ambient temperature using a static contact angle measurement (JC2000C, zhongchen, China). A drop of deionized water was dispensed on the sample, using a manual dispenser. Five measurements of the contact angle were taken across each sample, of which the average is reported.

Scanning electron microscopy (SEM) was carried out on a HITACHI S-5000 SEM to observe the fracture surface of the nanocomposites. All the samples were fractured in liquid nitrogen and the fracture surfaces were gold-plated.

DSC analysis was employed to examine the thermal transitions of the nanocomposites on a DSC instrument (Netzsch 200 F3) under nitrogen atmosphere. Samples were placed in sealed aluminum crucibles. All the samples were scanned over a range of −20 to 200°C (10°C/min for heating and 20°C/min for cooling) after a pretreatment of heating to 200°C and equilibrated at 200°C for 3 min to eliminate thermal and stress histories.

To better understand the crystallization behavior, P(3,4)HB and P(3,4)HB-based nanocomposites were studied by a polarized optical microscope (POM) equipped with a hot stage and a digital camera(Nikon model eclipse E400 pol). The samples were heated from room temperature to 200°C between two glass slides and equilibrated at this temperature for 2 min, then cooled rapidly to desired temperature and allowed to crystallize isothermally.

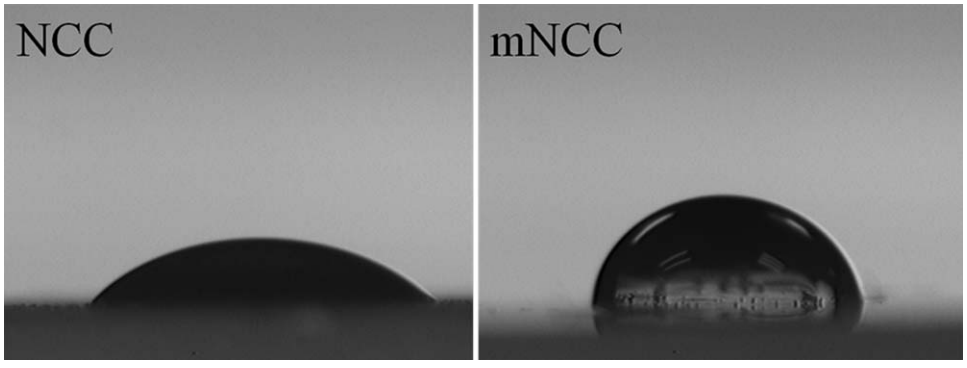

Figure 5. Contact angle pictures of water drop on NCC and mNCC films.

Applied Polymer SCIENCE

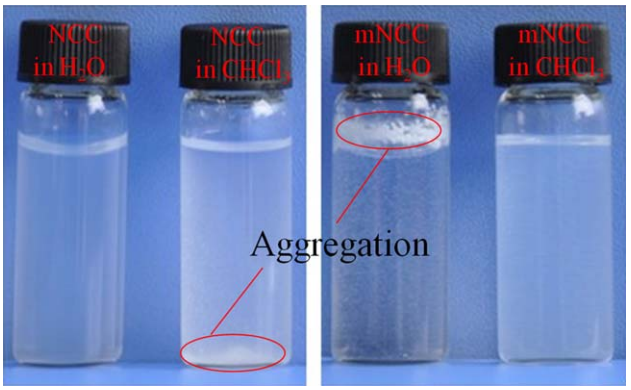

Figure 6. Pictures of nanocrystalline cellulose suspension in water and chloroform. [Color figure can be viewed in the online issue, which is available at wileyonlinelibrary.com.]

Dynamic mechanical analysis (DMA) of P(3,4)HB/mNCC nanocomposites was performed on a Perkin Elmer Pyris Diamond DMA dynamic mechanical analyzer in a temperature range of −40°C to 80°C at 5°C/min heating rate and 10 Hz constant frequency in the tensile configuration.

TGA was performed on a Q5000 IR thermogravimetric analyzer (TA Instruments) to determine the thermal stability of the nanocomposites. About 5 to 10 mg of samples was placed in a Pt pan and heated to 700°C at a heating rate of 20°C/min^{-1} under flowing nitrogen (60 mL/min^{-1}). Specimens were run in duplicate under the same condition and the average values are reported. The temperature is reproducible to ±1°C and the mass to ±0.2%.

RESULTS AND DISCUSSION

Preparation and Surface Modification of NCC

Figure 1(a) is the TEM image of NCC obtained by evaporating the water from aqueous suspension, which clearly shows that NCC possesses rod-like and nanoscale morphology with an average length of about 100 to 200 nm and diameter of about 10 nm.

Freeze-dried NCC was re-dispersed in DMF to obtain a stable suspension. Both the high value of the dielectric constant of DMF and the medium wettability of NCC are supposed to control the stability of NCC/DMF suspension.[25]

The chemical surface modification of NCC was carried out in DMF by homogeneous esterification after in-situ activation of lauric acid with Tos-Cl (Figure 2).[26–28] The FT-IR spectra for both NCC and mNCC are shown in Figure 3. Compared with NCC, the spectra of mNCC has two extra peaks at around 1251

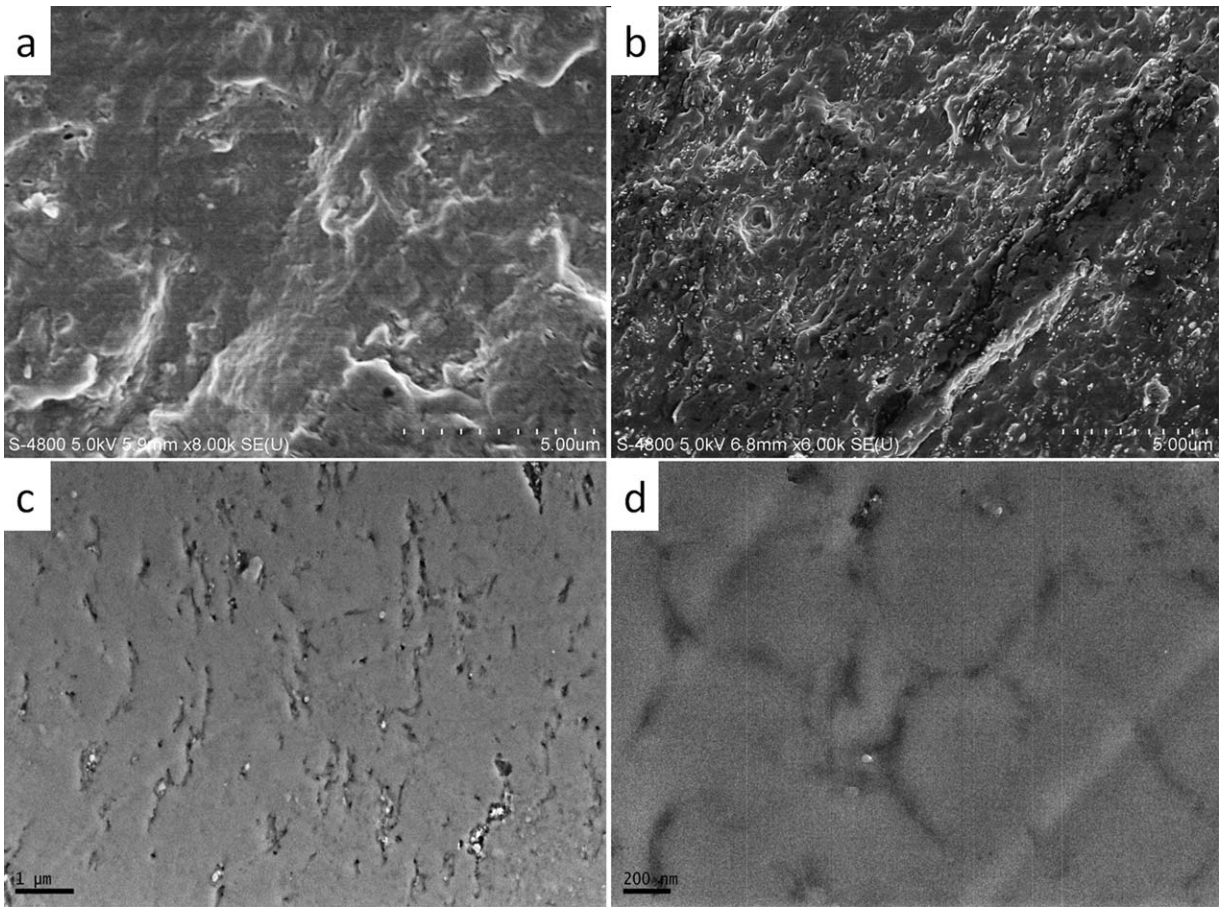

Figure 7. Micromorphology of the nanocomposites. (a) SEM micrograph of the fracture surface of neat P(3,4)HB; (b) SEM micrograph of the fracture surface of P(3,4)HB/1 wt % mNCC; (c) TEM image of P(3,4)HB/1 wt % mNCC nanocomposites at low magnification; (d) TEM image of P(3,4)HB/1 wt % mNCC nanocomposites at high magnification.

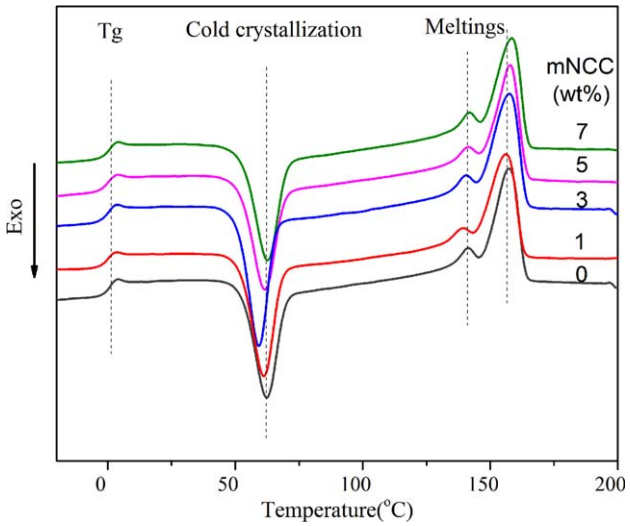

Figure 8. DSC thermograms of neat P(3,4)HB and P(3,4)HB/mNCC nanocomposites. [Color figure can be viewed in the online issue, which is available at wileyonlinelibrary.com.]

cm^{-1} and 1740 cm^{-1}, which attribute to the C-O-C and C=O vibration of the ester groups, respectively. Furthermore, obvious variation of C-H stretching vibration can be seen between 2850 cm^{-1} and 3000 cm^{-1}, which indicates that new grafting alkane is introduced on the surface of NCC. Meanwhile, the intensity of the broad band around 3300 cm^{-1} for mNCC decreases compared with NCC, which is due to the partial reacted hydroxyl. These changes confirm the success of the surface chemical modification on NCC.

The influence of surface modification on the morphology and crystallite structure of NCC was evaluated using TEM and XRD analysis. As shown in Figure 1(b), TEM images of NCC and mNCC all clearly present the rod-like character of nanoparticles. NCC seems to form bundle-like aggregates owing to the rich content of hydroxyl on its surface.[29] While mNCC has higher dispersity with the morphology maintained compared to NCC, which may be ascribed to the surface hydroxyl partially substituted and the weakened hydrogen bonding effect between the nanoparticles.

The XRD profile for mNCC is nearly identical to that of NCC (Figure 4), which indicates that NCC is chemically modified on the surface while the crystalline structure is not affected.

Contact-angle measurements were performed at ambient temperature using a dynamic drop tensiometer. Figure 5 shows the result of water contact angle measurement for a drop of water on the surfaces of NCC and mNCC films. Due to the OH-rich molecular structure, the NCC film is hydrophilic and gives a contact angle of 35°. However, after the surface modification, the hydrophobicity of mNCC is improved and the contact angle is up to 82°, illustrating that the surface hydroxyl group on NCC partially takes part in reaction and is replaced by the alkyl chain.

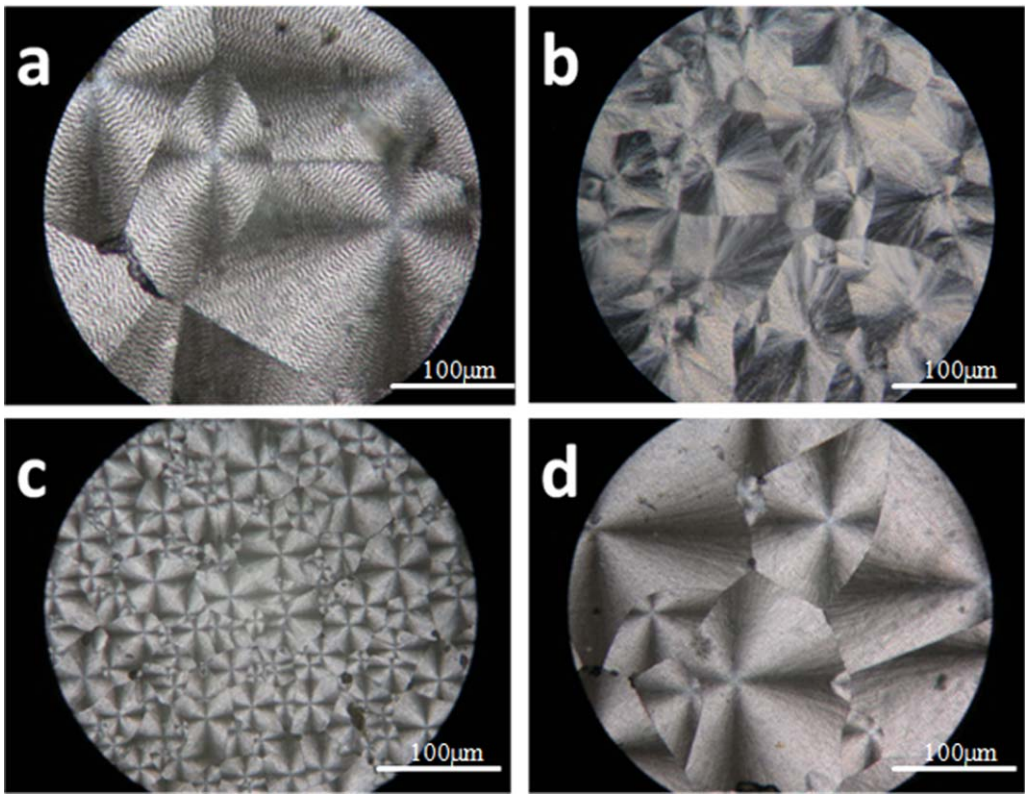

Figure 9. Polarizing optical microscope photographs of the P(3,4)HB and its nanocomposites. (a) Neat P(3,4)HB; (b) P(3,4)HB/1 wt % mNCC; (c) P(3,4)HB/3 wt % mNCC; (d) P(3,4)HB/5 wt % mNCC. [Color figure can be viewed in the online issue, which is available at wileyonlinelibrary.com.]

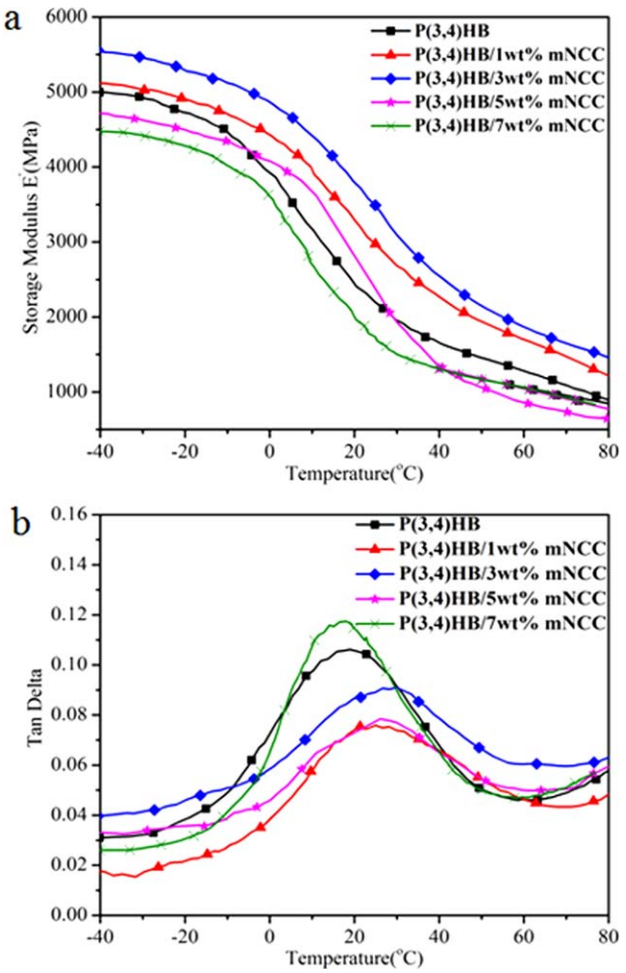

Figure 10. Storage modulus E' (a) and tan δ (b) as a function of temperature for neat P(3,4)HB and P(3,4)HB/mNCC nanocomposites. [Color figure can be viewed in the online issue, which is available at wileyonlinelibrary.com.]

NCC and mNCC were dispersed in water and chloroform respectively, and pictures of the suspension were collected several weeks later. As the pictures (Figure 6) show NCC can form stable aqueous suspension, but can not disperse in chloroform. While mNCC could disperse in chloroform homogeneously and can not form stable aqueous suspension. During the controlled sulfuric acid hydrolysis, sulfate ester groups and negative electrostatic charge were introduced onto the surface of NCC, which was responsible for the stability of NCC aqueous suspension. However, NCC can not be dispersed homogeneously in aprotic organic solvent (chloroform) owing to its hydrophilic surface. Compared with that of NCC, mNCC/chloroform suspension can remain stable for several weeks and no precipitation of the colloidal nanoparticles can be observed. This further demonstrates that the surface polarity of mNCC is improved effectively through esterification reaction.

Microstructure of P(3,4)HB/mNCC Nanocomposites

Whether the nanofillers could disperse uniformly in the matrix is one of the key factors to manufacture nanocomposites. The P(3,4)HB/mNCC nanocomposites with 1 wt % mNCC are employed to analyze the dispersity of mNCC in the matrix by comparing with the neat P(,4)HB. Shown in Figure 7(a,b) are SEM images of the fracture surface of neat P(3,4)HB and P(3,4)HB/1 wt % mNCC nanocomposites. Compared with the neat matrix [Figure 7(a)], the white dots in Figure 7(b) stand for the transversal sections of mNCC, which suggests that the nanofillers were well distributed in P(3,4)HB matrix. Figure 7(c,d) shows the TEM image of P(3,4)HB/1 wt % mNCC, from which the nanoscale and individual mNCC could be clearly seen and the size and morphology is the same as what is shown in Figure 1. The above results lead us to the conclusion that nanocomposites based on P(3,4)HB reinforced with mNCC are prepared successfully.

Crystallization Behavior of P(3,4)HB/mNCC Nanocomposites

DSC measurement was used to determine the thermal transition and crystallization behavior of P(3,4)HB and P(3,4)HB based nanocomposites. As shown in Figure 8, the glass transition, cold crystallization, and melting of P(3,4)HB can be clearly seen. Neat P(3,4)HB exhibits a glass transition ($T_{g,mid}$) at 0.5°C, an exothermic cold crystallization peak at 62°C and two endothermic melting peaks at 141 and 157°C, respectively. There is no significant variation of $T_{g,mid}$ of the nanocomposites with the addition of mNCC compared with that of neat P(3,4)HB. Similar phenomenon has been reported in other studies about nanocrystalline cellulose reinforced polymer composites.[30,31]

However, there is a significant decrease in cold crystallization temperature (T_c) when a small percentage of mNCC was added. This behavior is ascribed to the nucleation effect of the rigid fillers in P(3,4)HB matrix, which can reduce the energy barrier to form P(3,4)HB nuclei and facilitate P(3,4)HB cold crystallization. But when the content of mNCC is higher than 3 wt %, the value of T_c of the nanocomposites almost remain unchanged, implying that agglomeration of mNCC is formed. Excessive mNCC in the nanocomposites can prevent P(3,4)HB crystal growth and hinder the diffusion of P(3,4)HB chains to the growing crystallites.[32]

At the same time, a bimodal endothermic peak for all the samples around their melting point is observed, which demonstrates the melting-recrystallization-melting process.[30] The melting temperature of P(3,4)HB-based nanocomposites slightly shifts to high temperature when compared with that of neat P(3,4)HB. One of the factors for the increase of T_m in

Table I. Results for Dynamic Mechanical Analysis of Neat P(3,4)HB and P(3,4)HB/mNCC Nanocomposites

	Storage modulus (MPa)			
Sample code	−20°C	25°C	50°C	T_g (°C)
P(3,4)HB	4726	2194	1456	19
P(3,4)HB/1 wt % mNCC	4906	2970	1940	24
P(3,4)HB/3 wt % mNCC	5293	3485	2149	30
P(3,4)HB/5 wt % mNCC	4498	2373	1063	28
P(3,4)HB/7 wt % mNCC	4282	1732	1169	18

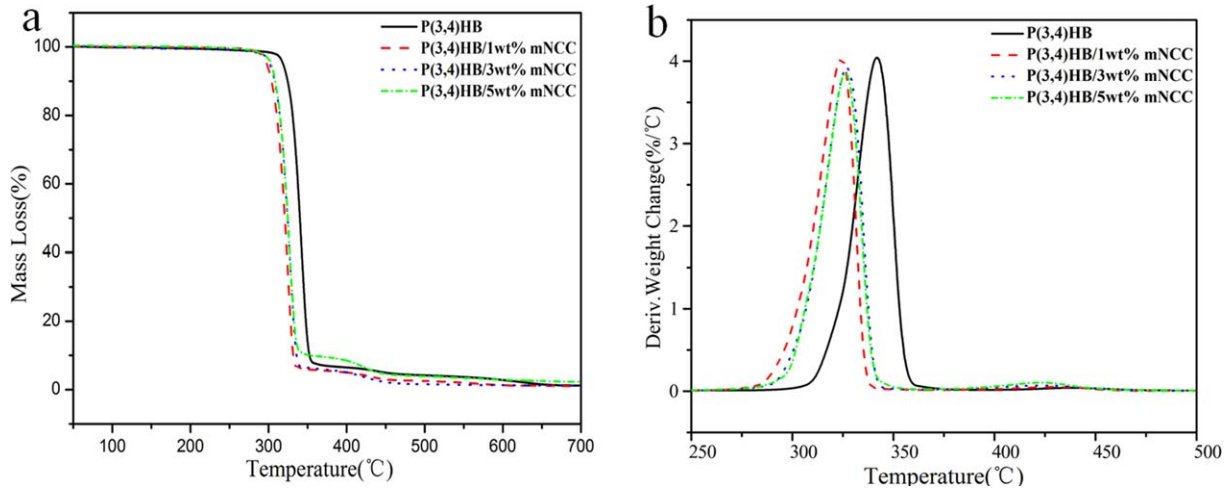

Figure 11. TGA (a) and DTG (b) curves for neat P(3,4)HB and P(3,4)HB/mNCC nanocomposites. [Color figure can be viewed in the online issue, which is available at wileyonlinelibrary.com.]

P(3,4)HB nanocomposites is that the presence of nanofillers facilitates the P(3,4)HB spherulite growth and leads to the formation of more perfect crystalline lamella.

The effect of mNCC on crystallization behavior of P(3,4)HB was further studied by POM observation. Figure 9 shows the POM photographs of P(3,4)HB and P(3,4)HB/mNCC nanocomposites. The Maltese cross of P(3,4)HB spherulites could be clearly seen under POM. It is obvious that with the incorporation of mNCC, the size of P(3,4)HB spherulites reduces and the number of P(3,4)HB spherulites increases significantly [shown in Figure 9(b,c)], which reveals that the nanoscale filler dispersed in the polymer matrix can act as a nucleating agent and promote P(3,4)HB crystallization. This is in agreement with the DSC results. But with the content of nanofiller increasing, the nucleation effect gradually decreases, which may be caused by the aggregation of mNCC [seen in Figure 9(d)].

Dynamic Mechanical Analysis of P(3,4)HB/mNCC Nanocomposites

Dynamic mechanical analysis (DMA) was carried out to characterize the reinforcing effect of mNCC in the nanocomposites at the frequency of 10 Hz. Figure 10 shows the trends of the dynamic storage modulus (E') and the loss tangent (tan δ), respectively, as a function of the temperature (ranging between −40°C and 80°C) for neat P(3,4)HB and P(3,4)HB/mNCC nanocomposites. The obtained data for storage modulus at different temperature and glass transition temperature (T_g) are summarized in Table I.

For all the samples from Figure 10(a) and Table I, it can be seen that as the temperature increases, especially nearby the glass transition temperature (T_g), the storage modulus decreases distinctly, which presents a typical behavior for a semicrystalline polymer.[33] The reinforcing effect of mNCC in P(3,4)HB matrix is significant. With the addition of 1 and 3 wt % mNCC, the storage modulus of nanocomposites at −20°C reaches 4906 MPa and 5293 MPa, respectively, with increment of about 4% and 12% in comparison with neat P(3,4)HB. And the increment rises up to 33% and 47% at 50°C, indicating that the reinforcing effect is more significant at the temperatures above the glass transition temperature (T_g). However, the reinforcement gradually decreases as the content of mNCC reaches 5 wt % or higher. It suggests that small amount of mNCC can disperse homogeneously in P(3,4)HB matrix and act as a efficient reinforcing agent, while at higher content level, mNCC in the matrix would aggregate and lose their reinforcing effect.

The tan δ, which is also called loss factor, reflects the damping of the materials. The peak of tan δ curve represents the α-relaxation and the corresponding temperature is referred to T_g. As shown in Figure 10(b), it can be seen that except for the sample with 7 wt % mNCC, T_g of the nanocomposites shift to higher temperature with small addition of mNCC. This result suggests that the segmental motion of the polymer chains along the two-phase interface is greatly restricted by the stiff rod-like nanofiller, which directly leading to the increment of T_g of P(3,4)HB.

Thermal Stability of P(3,4)HB/mNCC Nanocompoistes

The thermal stability and thermal decomposition of neat P(3,4)HB and its nanocomposites were investigated using TGA. Figure 11 shows the TGA and DTG curves for neat P(3,4)HB and P(3,4)HB/mNCC nanocompoistes. Table II gives the results of TGA and DTG for all samples. As shown in Figure 11(a) and Table II, one major weight loss step is observed in all samples. The addition of mNCC is found to slightly reduce the thermal

Table II. The Data of TGA and DTG for Neat P(3,4)HB and P(3,4)HB/mNCC Nanocomposites

Samples code	Onset degradation temperature (T_{onset}/°C)	DTG peak temperature (T_{max}/°C)	Ash content (%)
P(3,4)HB	314	342	0.7
P(3,4)HB/1 wt % mNCC	298	324	1.0
P(3,4)HB/3 wt % mNCC	302	327	1.2
P(3,4)HB/5 wt % mNCC	303	327	2.3

stability of the matrix polymer. With the nanofiller content increasing, the thermal decomposition onset temperature (T_{onset}, 3% mass loss) is decreased from 314°C for neat P(3,4)HB to 298, 302, and 303°C for P(3,4)HB/1 wt %, 3 wt %, 5 wt % mNCC nanocomposites, respectively. This may be caused by the heat conductivity effect of mNCC in the matrix.[34] As shown in the DTG curves [Figure 11(b)], the temperature at maximum mass loss rate (T_{max}) decreases with the weight percentage of mNCC increases, which is in agreement with the results of TGA. The minute peak occurring at 400°C in the composites is attributed to the decomposition of the nanofiller.

CONCLUSION

NCC is successfully modified by *in situ* activated esterification to prepare mNCC, which maintains similar morphology and microstructure to NCC. The mNCC obtained can disperse in chloroform and form stable colloidal suspension. P(3,4)HB/mNCC nanocompoistes are successfully prepared by solution casting method and well characterized. The results show that the mNCC can distribute individually in nanoscale in the matrix. With the addition of small amount of mNCC, the size of P(3,4)HB spherulites is reduced while the number of P(3,4)HB crystal particles increases significantly. The mechanical performances of P(3,4)HB/mNCC nanocompoistes are enhanced by 47% when 3 wt % mNCC is incorporated into P(3,4)HB compared with neat matrix, which may be ascribed to the uniform dispersion of mNCC in nanoscale in the matrix and the strong interfacial adhesion between mNCC and the matrix.

ACKNOWLEDGMENTS

The work was financially supported by the Natural Science Foundation of Jiangsu Province (BK2012821), the Project Funded by the Priority Academic Program Development (PAPD) of Jiangsu Higher Education Institutions, and the National Natural Science Foundation of China (50673078).

REFERENCES

1. Carli, L. N.; Crespo, J. S.; Mauler, R. S. *Compos. A* **2011**, *42*, 1601.
2. Lenz, R. W.; Marchessault, R. H. *Biomacromolecules* **2005**, *6*, 1.
3. Maiti, P.; Batt, C. A.; Giannelis, E. P. *Biomacromolecules* **2007**, *8*, 3393.
4. Cong, C. B.; Zhang, S. Y.; Xu, R. W.; Lu, W. C.; Yu, D. S. *J. Appl. Polym. Sci.* **2008**, *109*, 1962.
5. Zhang, R.; Huang, H.; Yang, W.; Xiao, X. F.; Hu, Y. *Compos. A* **2012**, *43*, 547.
6. Bondeson, D.; Mathew, A.; Oksman, K. *Cellulose* **2006**, *13*, 171.
7. Sturcova, A.; Davies, G. R.; Eichhorn, S. J. *Biomacromolecules* **2005**, *6*, 1055.
8. Lin, N.; Huang, J.; Chang, P. R.; Feng, J. W.; Yu, J. H. *Carbohydr. Polym.* **2011**, *83*, 1834.
9. Ljungberg, N.; Cavaille, J. Y.; Heux, L. *Polymer* **2006**, *47*, 6285.
10. Chazeau, L.; Cavaille, J. Y.; Ganova, G.; Dendievel, R.; Boutherin, B. *J. Appl. Polym. Sci.* **1999**, *71*, 1797.
11. Siqueira, G.; Bras, J.; Dufresne, A. *Biomacromolecules* **2009**, *10*, 425.
12. Lin, N.; Huang, J.; Chang, P. R.; Feng, J. W.; Yu, J. H. *Carbohydr. Polym.* **2011**, *83*, 1834.
13. Oksman, K.; Mathew, A. P.; Bondeson, D.; Kvien, I. *Compos. Sci. Technol.* **2006**, *66*, 2776.
14. Pei, A. H.; Malho, J. M.; Ruokolainen, J.; Zhou, Q.; Berglund, L. A. *Macromolecules* **2011**, *44*, 4422.
15. Ljungberg, N.; Bonini, C.; Bortolussi, F.; Boisson, C.; Heux, L.; Cavaille, J. Y. *Biomacromolecules* **2005**, *6*, 2732.
16. Majoinen, J.; Walther, A.; McKee, J. R.; Kontturi, E.; Aseyev, V.; Malho, J. M.; Ruokolainen, J.; Ikkala, O. *Biomacromolecules* **2011**, *12*, 2997.
17. Roy, D.; Guthrie, J. T.; Perrier, S. *Macromolecules* **2005**, *38*,10363.
18. Roman, M.; Winter, W. T. *ACS Symp. Ser.* **2006**, *938*, 99.
19. Stiubianu, G.; Cazacu, M.; Nicolescu, A.; Hamciuc, V.; Vlad, S. *J. Polym. Res.* **2010**, *17*, 837.
20. Raquez, J. M.; Murena, Y.; Goffin, A. L.; Habibi, Y.; Ruelle, B.; DeBuyl, F.; Dubois, P. *Compos. Sci. Technol.* **2012**, *72*, 544.
21. Lin, N.; Huang, J.; Chang, P. R.; Feng, J. W.; Yu, J. H. *Carbohydr. Polym.* **2011**, *83*, 1834.
22. Yuan, H. H.; Nishiyama, Y.; Wada, M.; Kuga, S. *Biomacromolecules* **2000**, *7*, 696.
23. Heux, L.; Chauve, G.; Bonini, C. *Langmuir* **2000**, *16*, 8210.
24. Petersson, L.; Kvien, I.; Oksman, K. *Compos. Sci. Technol.* **2007**, *67*, 2535.
25. Samir, M. A. S. A.; Alloin, F.; Sanchez, J. Y.; EI Kissi, N.; Dufresne, A. *Macromolecules* **2004**, *37*, 1386.
26. Sealey, J. E.; Samaranayake, G.; Todd, J. G.; Glasser, W. G. *J. Polym. Sci. Part B: Polym. Phys.* **1996**, *34*, 1613.
27. Heinze, T.; Schaller, J. *Macromol. Chem. Phys.* **2000**, *201*, 1214.
28. Heinze, T.; Liebert, T. F.; Pfeiffer, K. S.; Hussain, M. A. *Cellulose* **2003**, *10*, 283.
29. Araki, J.; Wada, M.; Kuga, S. *Langmuir* **2001**, *17*, 21.
30. Ten, E.; Turtle, J.; Bahr, D.; Jiang, L.; Wolcott, M. *Polymer* **2010**, *51*, 2652.
31. Samir, M. A. S. A.; Alloin, F.; Sanchez, J. Y.; Dufresne, A. *Polymer* **2004**, *45*, 4149.
32. Fornes, T. D.; Paul, D. R. *Polymer* **2003**, *44*, 4993.
33. Goffin, A. L.; Raquez, J. M.; Duquesne, E.; Siqueira, G.; Habibi, Y.; Dufresne, A.; Dubois, P. *Polymer* **2011**, *52*, 1532.
34. Shimazaki, Y.; Miyazaki, Y.; Takezawa, Y.; Nogi, M.; Abe, K.; Ifuku, S.; Yano, H. *Biomacromolecules* **2007**, *8*, 2976.